NMR Studies of the Exocyclic 1,N^6-Ethenodeoxyadenosine Adduct (ϵdA) opposite Thymidine in a DNA Duplex. Nonplanar Alignment of ϵdA(anti) and dT(anti) at the Lesion Site†

Michael Kouchakdjian,‡ Moises Eisenberg,§ Kevin Yarema,∥ Ashis Basu,∥ John Essigmann,*,∥ and Dinshaw J. Patel*,‡

Department of Biochemistry and Molecular Biophysics, College of Physicians and Surgeons, Columbia University, New York, New York 10032, Department of Pharmacological Sciences, State University of New York at Stony Brook, Stony Brook, New York 11794, and Department of Chemistry and Whitaker College of Health Sciences and Technology, Massachusetts Institute of Technology, Cambridge, Massachusetts 02139

Received September 6, 1990; Revised Manuscript Received October 29, 1990

ABSTRACT: Two-dimensional proton NMR studies are reported on the complementary d(C-A-T-G-T-G-T-A-C)·d(G-T-A-C-ϵA-C-A-T-G) nonanucleotide duplex (designated ϵdA·dT 9-mer duplex) containing 1,N^6-ethenodeoxyadenosine (ϵdA), a carcinogen–DNA adduct, positioned opposite thymidine in the center of the helix. Our NMR studies have focused on the conformation of the ϵdA·dT 9-mer duplex at neutral pH with emphasis on defining the alignment at the dT5·ϵdA14 lesion site. The through-space NOE distance connectivities establish that both dT5 and ϵdA14 adopt anti glycosidic torsion angles, are directed into the interior of the helix, and stack with flanking Watson–Crick dG4·dC15 and dG6·dC13 pairs. Furthermore, the d(G4-T5-G6)·d(C13-ϵA14-C15) trinucleotide segment centered about the dT5·ϵdA14 lesion site adopts a right-handed helical conformation in solution. Energy minimization computations were undertaken starting from six different alignments of dT5(anti) and ϵdA14(anti) at the lesion site and were guided by distance constraints defined by lower and upper bounds estimated from NOESY data sets on the ϵdA·dT 9-mer duplex. Two families of energy-minimized structures were identified with the dT5 displaced toward either the flanking dG4·dC15 or the dG6·dC13 base pair. These structures can be differentiated on the basis of the observed NOEs from the imino proton of dT5 to the imino proton of dG4 but not dG6 and to the amino protons of dC15 but not dC13 that were not included in the constraints data set used in energy minimization. Our NMR data are consistent with a nonplanar alignment of ϵdA14(anti) and dT5(anti) with dT5 displaced toward the flanking dG4·dC15 base pair within the d(G4-T5-G6)·d(C13-ϵA14-C15) segment of the ϵdA·dT 9-mer duplex.

Since its discovery as a carcinogen in humans (Creech & Johnson, 1974), vinyl chloride has been studied extensively [reviewed in Singer and Grunberger (1983) and Singer and Bartsch (1986)]. The mechanism of action of vinyl chloride involves its metabolic epoxidation to form chloroethylene oxide, which rearranges to form chloroacetaldehyde (Guengerich et al., 1979). Both compounds react with DNA to form a mixture of mono- and bifunctional adducts with the base residues (Osterman-Golkar et al., 1977; Scherer et al., 1981; Laib et al., 1981). The reaction of chloroacetaldehyde, which is a more stable compound than chloroethylene oxide, with deoxyadenosine and deoxycytidine results in an intermediate with an additional five-membered ring that undergoes dehydration to form 1,N^6-ethenodeoxyadenosine (ϵdA) and 3,N^4-ethenodeoxycytidine, respectively (Barrio et al., 1972; Kusmierek & Singer, 1982; Leonard, 1984). Deoxyguanosine forms analogous derivatives, and both 1,N^2- and N^2,3-ethenodeoxyguanosines have been isolated and characterized (Sattsangi et al., 1977; Singer et al., 1987).

The presence of the ϵdA adduct in vitro in rat liver RNA (Laib & Bolt, 1977) and in vivo in rat liver DNA (Green & Hathway, 1978) has been reported. It is thought that formation of the exocyclic etheno ring is unlikely to occur in hydrogen-bonded double-stranded DNA and that binding to the alkylating agents may occur only when the specific nucleophilic sites are accessible owing to thermal instability of the helix or during replication when single-stranded DNA segments are present (Singer & Grunberger, 1983).

The contribution of ϵdA to mutagenesis is unclear and continues to be investigated (Basu et al., 1987). Experiments have sought to test the role of ϵdA in directing the incorporation of erroneous bases during replication and transcription. Indeed, in vitro transcription studies have demonstrated that ϵdA misinserts ribonucleotides (Spengler & Singer, 1981). During in vitro replication by *Escherichia coli* DNA polymerase I, dG was misincorporated opposite a chloroacetaldehyde-treated poly(dA) template (Barbin et al., 1981). Hall et al. (1981) also found that dG and dC preferentially incorporated in DNA treated with chloroacetaldehyde. More recently, however, attempts have been made to quantify ϵdA misincorporation by using in vitro replication and transcription systems (Singer et al., 1984; Singer & Spengler, 1986). These studies confirmed that dG is misinserted on replication but at a much lower frequency than previously reported. The authors suggest that ϵdA generally does not prevent dT incorporation but behaves as a bulky lesion that could be bypassed, thus possibly causing a frame-shift mutation.

In order to elucidate the error-free bypass and the mispairing alternatives of the ϵdA exocyclic adduct **1**, our laboratories have undertaken structural studies of the etheno-dA lesion

† This research was supported by NIH Grant CA-49982 to D.J.P. and NIH Grant CA-52127 to J.E.

‡ Columbia University.
§ State University of New York at Stony Brook.
∥ Massachusetts Institute of Technology.

0006-2960/91/0430-1820$02.50/0

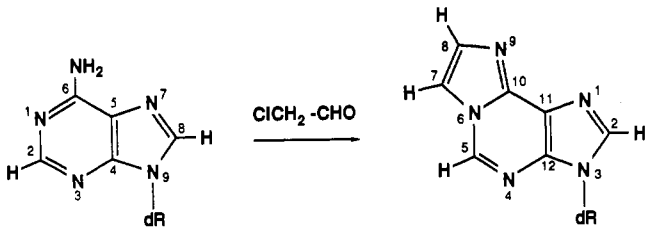

1

(designated ϵdA) opposite dT and dG in short oligonucleotide duplex segments. This contribution focuses on two-dimensional proton NMR and energy minimization studies of the d(C-A-T-G-T-G-T-A-C)·d(G-T-A-C-ϵA-C-A-T-G) nonanucleotide duplex (designated ϵdA·dT 9-mer, **2**), which contains a dA exocyclic adduct, ϵdA, positioned opposite thymidine in the center of the helix.

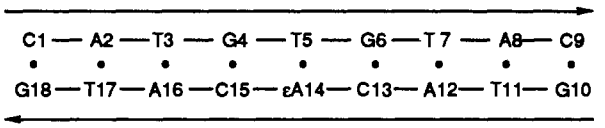

2

Experimental Procedures

Oligonucleotide Synthesis. The deoxyoligonucleotide containing etheno-dA was prepared from the protected monomer, 5′-*O*-(4,4′-dimethoxytrityl)-3-(2-deoxy-D-*erythro*-pentofuranosyl)imidazo[2,1-*i*]purine 3′-[2-cyanoethyl *N*,*N*-diisopropylphosphoramidite]. The ϵdA deoxyribonucleoside was synthesized according to the literature procedure (Secrist et al., 1972). A dimethoxytrityl group was introduced on the 5′-hydroxyl (Basu et al., 1987), and the phosphitylation at the 3′-hydroxyl was carried out with 2-cyanoethyl *N*,*N*,*N*′,*N*′-tetraisopropylphosphorodiamidite in acetonitrile in the presence of tetrazole and diisopropylamine (Gaffney & Jones, 1989). The oligodeoxynucleotide d(G-T-A-C-ϵA-C-A-T-G) was synthesized on a 10-μmol scale on an Applied Biosystems Model 381A automated synthesizer by the cyanoethyl phosphoramidite method (Gait, 1984). Because of the unstable nature of ϵdA, the capping step during synthesis was omitted, and deprotection was carried out in the presence of 1,8-diazabicyclo[5.4.0]undec-7-ene as previously reported (Basu et al., 1987). The deprotected oligodeoxynucleotide was purified by HPLC on an Alltech Spherisorb SAX column (250 × 4.6 mm) eluted with a gradient of 0.2-1.0 M monobasic potassium phosphate in 5% methanol over a period of 40 min. Nucleoside composition analysis performed as described (Basu et al., 1987) was consistent with the sequence of the 9-mer.

Sample Preparation. A 1:1 stoichiometric ratio of the ϵdA-containing strand and the complementary strand was achieved by monitoring the intensities of the base protons on addition of the unmodified strand to the lesion-containing strand at 45 °C. NMR experiments were performed on ϵdA·dT 9-mer duplex preparations containing 0.1 M NaCl, 10 mM phosphate, and 1 mM EDTA in 0.4 mL of either 100% D_2O or 90% H_2O/10% D_2O (v/v). Samples containing 250 A_{260} units of the ϵdA·dT 9-mer duplex were used for two-dimensional experiments in D_2O solution while 400 A_{260} units of duplex were used in two-dimensional experiments in H_2O solution. The pH values in D_2O are uncorrected pH meter readings.

NMR Experiments. Proton NMR experiments were performed on a Bruker AM 500 spectrometer while phosphorus NMR experiments were performed on an AM 300 spectrometer. Proton chemical shifts are referenced relative to external sodium 3-(trimethylsilyl)propionate-*2,2,3,3-d*$_4$ (TSP) while phosphorus chemical shifts are referenced relative to external trimethyl phosphate (TMP).

Pulse sequences, data accumulation, and processing parameters for one- and two-dimensional NMR experiments in both H_2O and D_2O solution are similar to those reported previously (Kouchakdjian et al., 1989, 1990). All data sets were processed by use of FTNMR software on a micro VAXII computer.

Energy Minimization. Interproton distance constraints defined by lower and upper bounds were obtained by measuring the NOE cross peak volume integrals of the ϵdA·dT 9-mer duplex at mixing times of 50, 80, and 250 ms. First, a standard B-form 9-mer duplex was constructed that had the sequence d(C1-A2-T3-G4-T5-G6-T7-A8-C9)·d(G10-T11-A12-C13-A14-C15-A16-T17-G18). The adenine base at position 14 was modified to incorporate the etheno bridge to generate the 1,N^6-ethenoadenine base. The ϵdA14 with the added exocyclic ring cannot fit without clashing opposite dT5 when both bases adopt anti glycosidic torsion angles in the standard B-form DNA. In order to relieve this steric clash, six different starting models were used which take into account the various positioning possibilities of the ϵdA adduct opposite thymidine at the lesion site but keep the rest of the DNA molecule very close to the original B-form.

These starting structures were energy minimized by use of the program XPLOR on a Convex C220 minisupercomputer. The interproton distances defined by lower and upper bounds estimated from the NOE cross peak volume integrals were used as distance restraints. Minimization parameters were similar to those described previously (Kouchakdjian et al., 1990).

Results

The numbering system of the ϵdA ring shown in **1** differs from that used for unmodified purine rings. Thus, the purine H8 proton is labeled H2 in ϵdA, and the purine H2 proton is labeled H5 in ϵdA.

The exchangeable proton spectrum (7.0–14.0 ppm) at 5 °C (Figure 1A), nonexchangeable proton spectrum (5.5–8.2 ppm) at 15 °C (Figure 1B), and phosphorus spectrum (−3.0 to −5.0 ppm) at 15 °C (Figure 1C) of the ϵdA·dT 9-mer duplex at pH 7.0 establish the formation of a stable conformation of the nonanucleotide duplex, which contains an ϵdA exocyclic lesion positioned opposite thymidine in the center of the duplex.

Exchangeable Protons. The exchangeable proton spectrum (6.0–14.5 ppm) of the ϵdA·dT 9-mer duplex in H_2O buffer, pH 7.0 at 5 °C (Figure 1A), displays well-resolved thymidine imino protons at chemical shifts between 13.5 and 13.7 ppm and deoxyguanosine imino protons between 11.8 and 12.8 ppm. Exchangeable amino protons and nonexchangeable base protons resonate between 6.4 and 8.8 ppm. An additional exchangeable resonance is detected at 11.10 ppm in Figure 1A.

Exchangeable proton resonances were assigned by analyzing the cross peaks in a 120-ms mixing time NOESY spectrum of the ϵdA·dT 9-mer duplex in H_2O buffer, pH 7.0 at 5 °C. Expanded contour plots of this spectrum establishing the distance connectivities between the imino protons (11.5–14.0 ppm) and the base and amino protons (6.0–9.0 ppm) are plotted in Figure 2A, and connectivities between the symmetrical imino proton region (11.5–14.0 ppm) are plotted in Figure 2B. We detect NOE cross peaks between thymidine imino and deoxyadenosine H2 protons within each of the four dA·dT base pairs (peaks A–D, Figure 2A) and between deoxyguanosine imino and hydrogen-bonded (peaks F and H, Figure 2A) and exposed (peaks G and I, Figure 2A) deoxy-

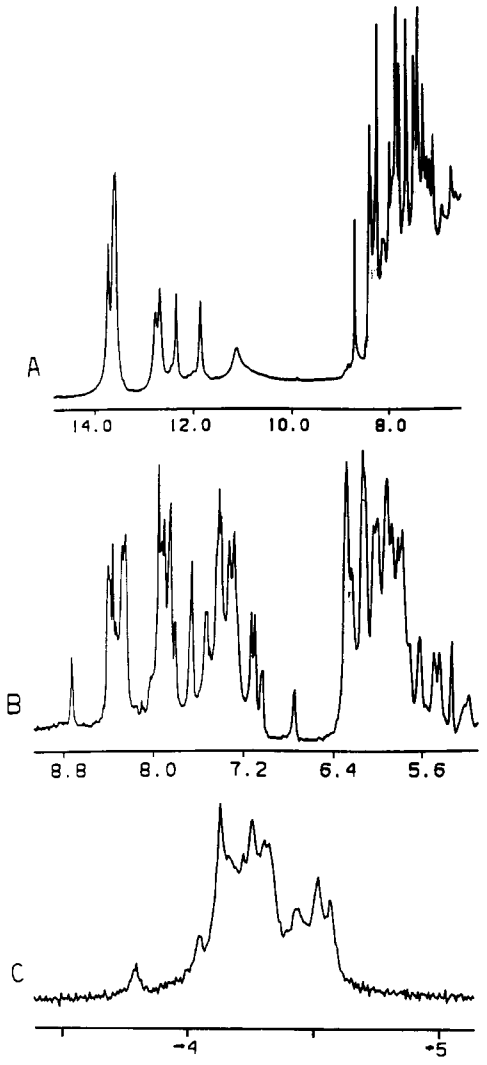

FIGURE 1: (A) Exchangeable proton spectrum (6.0–15.0 ppm) at 5 °C, (B) nonexchangeable proton spectrum (5.2–9.0 ppm) at 15 °C, and (C) proton-decoupled phosphorus spectrum (−3.5 to −5.0 ppm) at 15 °C of the ϵdA·dT 9-mer duplex in 0.1 M NaCl and 10 mM phosphate, aqueous solution, pH 7.0.

cytidine amino protons within the nonterminal dG·dC base pairs in the ϵdA·dT 9-mer duplex.

The imino protons were assigned as outlined below. The nonexchangeable H5 protons of dC13 and dC15 were independently assigned following analysis of NOESY spectra of the ϵdA·dT 9-mer duplex in D_2O solution (see following section). We detect NOEs from the deoxyguanosine imino protons to the hydrogen-bonded and exposed deoxycytidine amino protons, which in turn exhibit NOEs to the deoxycytidine H5 protons within individual dG·dC base pairs. This permits differentiation and assignment of the imino protons of the dG6·dC13 and dG4·dC15 base pairs in the ϵdA·dT 9-mer duplex. In addition, NOEs are detected between the imino protons on adjacent dG4·dC15 and dT3·dA16 base pairs (peak A, Figure 2B) and between the imino protons on adjacent dG6·dC13 and dT7·dA12 base pairs (peak B, Figure 2B) in the ϵdA·dT 9-mer duplex.

The nonexchangeable H2 protons of dA2 and dA16 were independently assigned following analysis of NOESY spectra of the ϵdA·dT 9-mer duplex in D_2O solution. This permits differentiation and assignment of the imino protons in dA2·dT17 and dA8·dT11 based on the observed NOEs from the assigned deoxyadenosine H2 protons to the imino protons of their thymidine partners across the base pair. The chemical

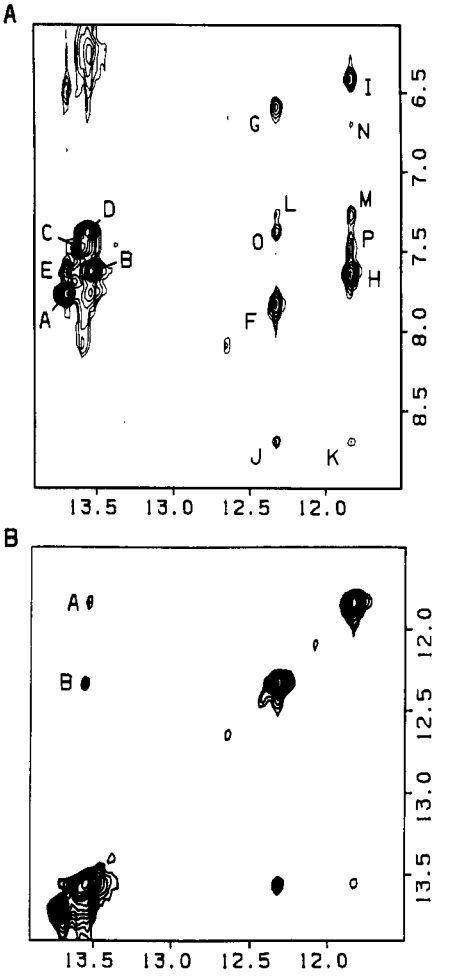

FIGURE 2: Expanded contour plots of the NOESY spectrum (mixing time 120 ms) of the ϵdA·dT 9-mer duplex in 0.1 M NaCl and 10 mM phosphate, H_2O, pH 7.0 at 5 °C. (A) NOE cross peaks establishing connectivities between the 11.5–14.0 ppm imino proton region and the 6.0–9.0 ppm base and amino proton region. Cross peaks A–P are assigned as follows: A, T17(imino)–A2(H2); B, T3(imino)–A16(H2); C, T11(imino)–A8(H2); D, T7(imino)–A12(H2); E, T17(imino)–A16(H2); F and G, G6(imino)–C13(H4,h/e); H and I, G4(imino)–C15(H4,h/e); J, G6(imino)–ϵA14(H5); K, G4(imino)–ϵA14(H5); L, G6(imino)–ϵA14(H7); M, G4(imino)–ϵA14(H7); N, G4(imino)–ϵA14(H8); O, G6(imino)–A12(H2); P, G4(imino)–G4(H2h). The symbols h and e stand for hydrogen-bonded and exposed amino protons, respectively, involved in Watson–Crick pairing. (B) NOE cross peaks establishing connectivities in the symmetrical 11.5–14.0 ppm imino proton region. The cross peaks A and B are assigned as follows: A, T3(imino)–G4(imino); B, G6(imino)–T7(imino).

Table I: Exchangeable Proton Chemical Shifts in the ϵdA·dT 9-mer Duplex at 5 °C[a]

	chemical shift (ppm)			
base pair	T(NH3)	G(NH1)	C(NH_2-4)[b]	A(H2)
C1·G18		12.72		
A2·T17	13.69			7.76
T3·A16	13.53			7.62
G4·C15		11.83	7.64, 6.41	
T5·ϵA14	11.10			
G6·C13		12.32	7.83, 6.59	
T7·A12	13.55			7.30
A8·T11	13.58			7.47
C9·G10		12.64	8.08	

[a] 0.1 M NaCl, 10 mM phosphate, H_2O, pH 7.0. [b] Hydrogen-bonded cytidine amino proton downfield from exposed cytidine amino proton.

shifts of the imino, amino, and deoxyadenosine H2 protons for the ϵdA·dT 9-mer duplex in H_2O buffer at 5 °C are listed in Table I.

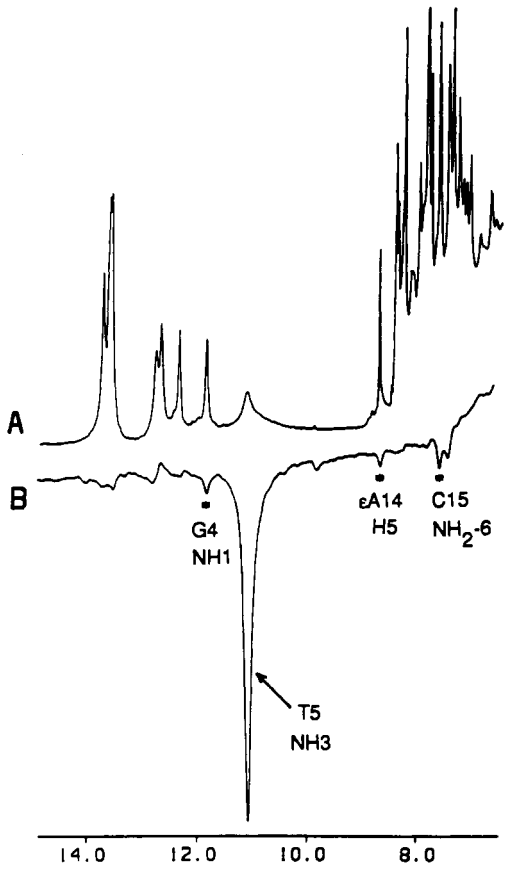

FIGURE 3: (A) Exchangeable proton spectrum (6.0–15.0 ppm) of the ϵdA·dT 9-mer duplex in 0.1 M NaCl and 10 mM phosphate, H_2O, pH 7.0 at 5 °C. (B) One-dimensional NOE difference spectrum following 0.4-s saturation of the 11.10 ppm resonance.

The orientation of the ϵdA adduct can be characterized from the observed NOEs between the 12.32 guanosine imino proton of the dG6·dC13 pair and the 8.72 ppm H5 proton (peak J, Figure 2A) and the 7.32 ppm H7 proton (peak L, Figure 2A) of ϵdA14 in the duplex. A similar set of NOEs are detected between the 11.83 ppm deoxyguanosine imino proton of the dG4·dC15 pair and the H5 (peak K, Figure 2A), H7 (peak M, Figure 2A), and H8 (peak N, Figure 2A) protons of ϵdA14 in the duplex.

We did not detect an NOE cross peak between the remaining exchangeable resonance at 11.10 ppm and other protons in the NOESY experiment since this somewhat broadened resonance exchanges with H_2O during the 120-ms mixing time, thereby reducing its intensity considerably. The line shape and area of this 11.10 ppm exchangeable resonance is dependent on temperature and pH.

We have attempted to record one-dimensional NOE difference spectra following irradiation of the 11.10 ppm imino proton resonance in the ϵdA·dT 9-mer duplex as a function of pH and temperature, but the data and interpretations are not definitive. We detect weak NOEs at the 11.83 ppm imino proton of dG4, the 8.68 ppm H5 proton of ϵdA14, and the 7.60 ppm hydrogen-bonded amino proton of dC15 following 0.1-s irradiation of the 11.10 ppm proton in the ϵdA·dT 9-mer duplex in H_2O buffer, pH 7.0 at 5 °C (Figure 3B). These data require that the 11.10 ppm resonance be assigned to the imino proton of dT5 opposite the ϵdA14 lesion site in the ϵdA·dT 9-mer duplex.

The dT5·ϵdA14 lesion site is flanked by the dG4·dC15 and dG6·dC13 base pairs in the ϵdA·dT 9-mer duplex. We note that the imino proton of dG4 broadens and shifts downfield while the imino proton of dG6 is unaffected on lowering the pH of the ϵdA·dT 9-mer duplex from pH 7.0 to pH 5.2 at 5 °C (Figure S1, supplementary material). The 11.10 ppm exchangeable resonance exhibits a broad and narrow component at pH 7.0, 5 °C, with an intensity greater than one proton (Figure S1A). The relative intensity of this resonance increases further on lowering the pH to 5.2 at 5 °C (Figure S1B).

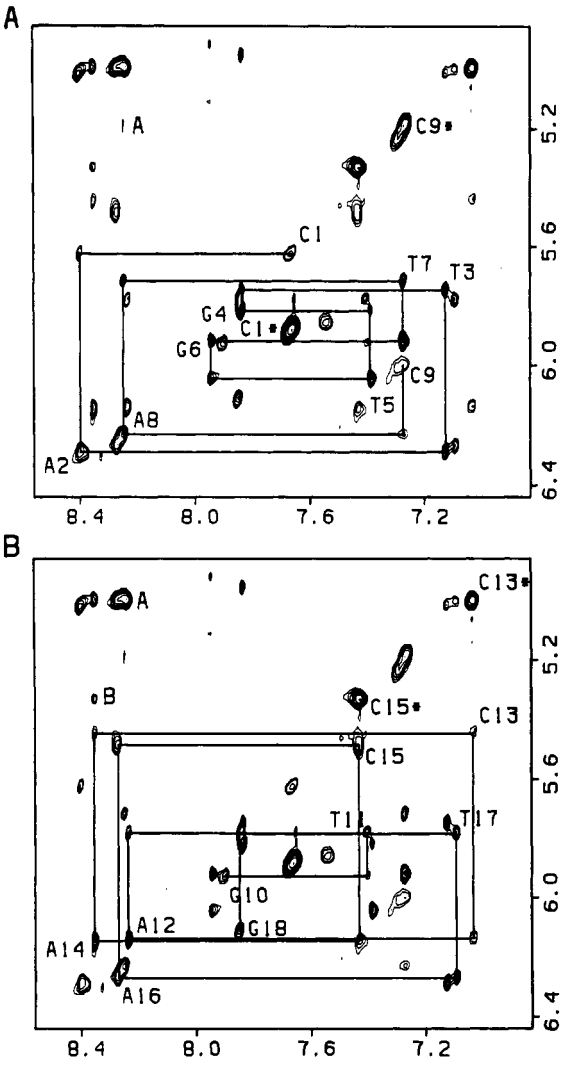

FIGURE 4: Expanded duplicate contour plots of the NOESY spectrum (250-ms mixing time) of the ϵdA·dT 9-mer duplex in 0.1 M NaCl and 10 mM phosphate, D_2O, pH 7.0 at 15 °C. This region establishes distance connectivities between the base protons (6.8–8.5 ppm) and the sugar H1′ and deoxycytidine H5 protons (4.8–6.4 ppm). The chain is traced from C1 to C9 in (A) and from G10 to G18 in (B). The tracing follows connectivities between adjacent base protons through their intervening sugar H1′ protons. The deoxycytidine H5–H6 cross peaks are designated by asterisks.

Nonexchangeable Protons. The nonexchangeable proton spectrum (5.4–8.8 ppm) of the ϵdA·dT 9-mer duplex in D_2O buffer, pH 7.0 at 15 °C, is shown in Figure 1B. The contour plot of the 250-ms mixing time NOESY spectrum of the ϵdA·dT 9-mer duplex in D_2O buffer, pH 7.0 at 15 °C, is plotted in Figure S2A (supplementary material) and exhibits well-resolved cross peaks. An expanded region of the 250-ms NOESY contour plot establishing distance connectivities between the base protons (6.8–8.6 ppm) and the sugar H1′ and deoxycytidine H5 protons (4.8–6.4 ppm) is shown in duplicate in Figure 4. The purine H8 and pyrimidine H6 protons exhibit NOEs to their own and 5′-flanking sugar H1′ protons (Hare et al., 1983) such that the oligonucleotide chain can be traced without interruption for both the unmodified d(C1-A2-T3-G4-T5-G6-T7-A8-C9) strand (Figure 4A) and the

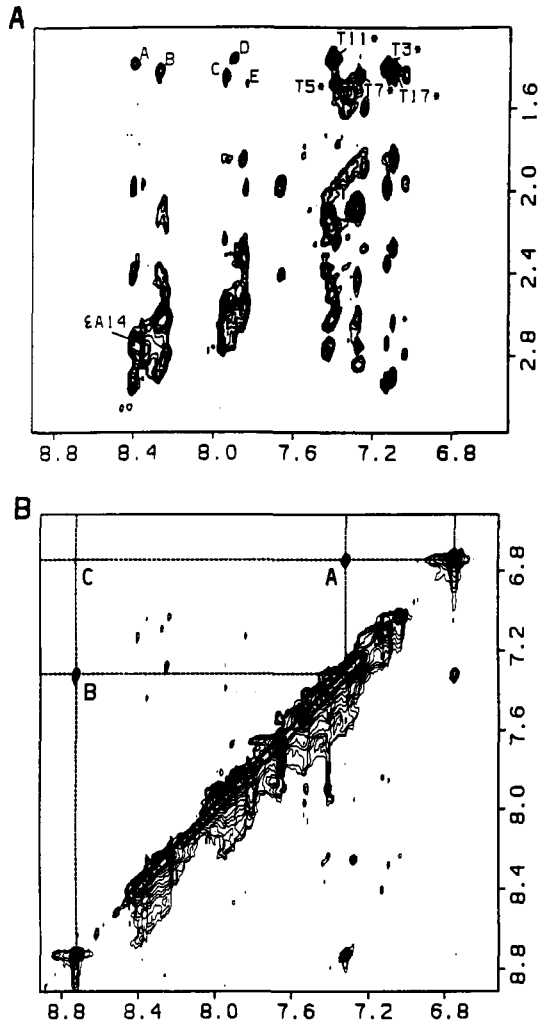

FIGURE 5: Expanded contour plots of the NOESY spectrum (250-ms mixing time) of the εdA·dT 9-mer duplex in 0.1 M NaCl and 10 mM phosphate, D_2O, pH 7.0 at 15 °C. (A) This region establishes distance connectivities between the base proton (6.4–9.0 ppm) and the sugar H2′,2″ proton (1.2–3.2 ppm) region. Cross peaks A–E are assigned as follows: A, A2(H8)–T3(CH_3); B, A16(H8)–T17(CH_3); C, G6(H8)–T7(CH_3); D, G10(H8)–T11(CH_3); E, G4(H8)–T5(CH_3). The thymidine H6-CH_3 NOE cross peaks are designated by asterisks. (B) This region establishes distance connectivities in the symmetrical 6.4–9.0 ppm base proton region. Cross peaks A–C are assigned as follows: A, εA14(H7)–εA14(H8); B, εA14(H5)–εA14(H7); C, εA14(H5)–εA14(H8).

lesion-containing d(G10-T11-A12-C13-εA14-C15-A16-T17-G18) strand (Figure 4B). The NOE cross peak intensities between the base protons and their own sugar H1′ protons for dT5 (Figure 4A) and εdA14 (Figure 4B) are of the same order of magnitude as those between other bases to their own sugar H1′ protons in the NOESY contour plot of the εdA·dT 9-mer duplex (Figure 4). These observations are confirmed in NOESY spectra recorded at a shorter mixing time of 50 ms and establish that no base to its own sugar H1′ NOE is of comparable intensity to the NOE between the H6 and H5 protons of cytidine (Figure S2B).

We detect NOE cross peaks between protons within the εdA in the expanded NOESY contour plot of the symmetrical 6.6–8.8 ppm base proton region. A strong cross peak is detected between the 6.75 ppm H8 proton and 7.32 ppm H7 proton of εdA14 (peak A, Figure 5B) while the downfield-shifted 8.72 ppm H5 proton of εdA14 exhibits a strong NOE to the H7 proton (peak B, Figure 5B) and a weak NOE to the H8 proton (peak C, Figure 5B) of εdA14 in the εdA·dT 9-mer duplex.

Table II: Nonexchangeable Proton Chemical Shifts in the εdA·dT 9-mer Duplex at 15 °C[a]

	chemical shift (ppm)							
base	H8	H2	H6	H5/CH_3	H1′	H2′	H2″	H3′
C1			7.66	5.88	5.62	1.97	2.41	4.69
A2	8.40	7.81			6.29	2.74	2.94	5.02
T3			7.13	1.39	5.75	1.99	2.36	
G4	7.83				5.81	2.55	2.57	
T5			7.39	1.49	6.04	2.25	2.60	
G6	7.94				5.92	2.59	2.75	
T7			7.27	1.45	5.71	2.09	2.43	
A8	8.25				6.23	2.63	2.85	4.99
C9			7.27	5.19	6.00	2.07	2.10	
G10	7.90				5.93	2.62	2.74	4.79
T11			7.40	1.36	5.78	2.18	2.50	
A12	8.23				6.13	2.63	2.79	5.00
C13			7.03	5.00	5.44	1.44	1.97	4.69
C15			7.43	5.33	5.49	2.12	2.39	4.80
A16	8.27	7.64			6.27	2.64	2.90	4.99
T17			7.09	1.42	5.78	1.84	2.28	4.82
G18	7.85				6.11	2.33	2.58	4.66

lesion	H2	H5	H7	H8	H1′	H2′	H2″	H3′
εA14	8.35	8.72	7.32	6.75	6.15	2.78	2.65	5.00

[a] 0.1 M NaCl, 10 mM phosphate, D_2O, pH 7.0.

We did not detect any NOE cross peaks between the resolved 8.72 ppm H5 proton of εdA14 and sugar protons (the H2′,2″ proton region is plotted in Figure 5A) in the εdA·dT 9-mer duplex (Figure 5A).

Other expanded regions of the NOESY data set, as well as the COSY data set, were analyzed to complete and confirm the nonexchangeable base and sugar H1′, H2′, and H2″ proton assignments in the εdA·dT 9-mer duplex, and these proton chemical shifts are listed in Table II.

Phosphorus Spectra. The proton-decoupled phosphorus spectrum of the εdA·dT 9-mer duplex in D_2O, pH 7.0 at 15 °C, is plotted in Figure 1C. The phosphorus resonances are somewhat broad and are dispersed between −3.8 to −4.6 ppm. We have been unable to assign the phosphorus resonances due to the limited resolution of the εdA·dT 9-mer duplex spectrum.

Energy Minimization. The NMR parameters are consistent with εdA14 and dT5 at the lesion site adopting anti glycosidic torsion angles in the εdA·dT 9-mer duplex, and therefore, our starting structures (six in number) were variants of this alignment at the lesion site. The first of the six starting structures, Init 1, makes no attempt to relieve the steric clash. εdA14 is opposite dT5 as it would have been for a standard dA·dT pair. The remaining five structures were built as follows: for the Init 2 starting structure, both εdA14 and dT5 are moved away from each other in the direction perpendicular to the helix axis while at the same time keeping dT5 and εdA14 in the base pair plane. This represents a slightly bulged out structure at the lesion site. For the Init 3 starting structure, dT5 swings toward the minor groove and εdA14 toward the major groove, while for the Init 4 starting structure, dT5 swings toward the major groove and εdA14 toward the minor groove. The dT5 and εdA14 bases are deflected toward their 5′ neighbors in the Init 5 structure, and the dT5 and εdA14 are deflected toward their 3′ neighbors in the Init 6 structure. These last five structures, Init 2–6, represent the five different directions in which to move εdA14 and dT5 in order to relieve the steric clash that would occur at the lesion site in a strict B-form DNA structure. In all of these cases, only minor structural variations of the DNA backbone and the two base pairs flanking the lesion site were required to generate the starting structures.

Distance bounds for the εdA·dT 9-mer were established by measuring the volume integrals of NOE cross peaks relative

Table III: Proton–Proton Distance Constraints in the d(G4-T5-G6)·d(C13-ϵA14-C15) Segment of the ϵdA·dT 9-mer Duplex[f]

	intraresidue constraints on the same strand (Å)				
	base–H1′	base–H2′	base–H2″	H1′–H2′	H1′–H2″
G4	2.1–3.9[d]	a	a	a	a
T5	3.4–4.8[c]	2.0–3.3[c]	3.0–4.4[c]	2.4–3.8[c]	2.1–2.5[c]
G6	2.2–4.0[d]	a	2.7–4.1[c]	2.3–3.7[c]	a
C13	2.5–4.3[d]	1.0–3.5[c]	2.8–4.0[c]	b	2.0–3.3[c]
ϵA14	2.1–3.9[d]	2.0–3.0[c]	2.7–4.5[d]	a	a
C15	2.2–4.0[d]	2.0–3.0[c]	2.2–3.6[c]	2.7–4.0[d]	2.1–3.5[c]

	interresidue constraints on the same strand (Å)				
	H1′–base	H2′–base	H2″–base	base–CH_3	H1′–CH_3
G4–T5	2.6–4.4[d]	a	a	2.4–4.7[c]	2.1–4.4[d]
T5–G6	2.2–4.0[d]	2.7–4.1[c]	a		
C13–ϵA14	2.5–4.3[d]	b	2.5–3.9[c]		
ϵA14–C15	2.2–4.0[d]	a	a		

	interresidue constraints on partner strands (Å)		
	ϵA14(H5)	ϵA14(H8)	ϵA14(H7)
G4(NH1)	2.0–4.9[e]	2.1–5.1[e]	2.0–4.5[e]
G6(NH1)	2.0–4.8[e]	b	2.0–4.9[e]

[a] Overlap. [b] Very weak or absent. [c] 50- and 80-ms NOESY data in D_2O. [d] 250-ms NOESY data in D_2O. [e] 120-ms NOESY data in H_2O. [f] Base: H6 protons for pyrimidines, H8 protons for purines, and H2 proton for ϵdA14.

to reference cross peaks corresponding to the H5-H6 protons of cytidine (fixed distance of 2.45 Å) at mixing time values of 50, 80, and 250 ms. The estimated distances were given lower and upper bounds of −0.6 and +0.8 Å for the NOESY data set collected at mixing times of 50 and 80 ms and lower and upper bounds of −0.8 and +1.0 Å for the NOESY data set collected at a mixing time of 250 ms. The NOE distance constraints defined by lower and upper bounds for the d-(G4-T5-G6)·d(C13-ϵA14-C15) segment are tabulated in Table III. A total of 136 distance bounds for the ϵdA·dT 9-mer duplex were incorporated as square-well potential constraints in the energy minimization algorithm of the XPLOR program. All six structures were energy minimized with the NOE-derived distances as constraints. Five of these converged to conformations that were very similar to each other (designated energy-minimized structure I) with dT5 displaced toward the flanking dG6·dC13 pair. The remaining starting structure, Init 5, in which dT5 and ϵdA14 are deflected toward their 5′ neighbors resulted, following energy minimization, in structure II, with dT5 retaining its displacement toward the dG4·dC15 base pair.

The energy-minimized d(G4-T5-G6)·d(C13-ϵA14-C15) segment of structure I with dT5 displaced toward the flanking dG6·dC13 base pair is shown in stereo in Figure S3A (supplementary material). A stereoview of the alignment of dT5 and ϵdA14 at the lesion site as viewed down the helix axis is plotted in Figure S3B. The relevant interproton distances for the d(G4-T5-G6)·d(C13-ϵA14-C15) segment from the energy-minimized structure I are listed in Table IV.

The corresponding stereoviews and interproton distances for the d(G4-T5-G6)·d(C13-ϵA14-C15) segment of energy-minimized structure II with dT5 displaced toward the flanking dG4·dC15 base pair are plotted in Figure 6 and listed in Table V, respectively.

Table IV: Proton–Proton Distances in the d(G4-T5-G6)·d(C13-ϵA14-C15) Segment for the Energy-Minimized Structure I of the ϵdA·dT 9-mer Duplex[a]

	intraresidue distances on the same strand (Å)				
	base–H1′	base–H2′	base–H2″	H1′–H2′	H1′–H2″
G4	3.9	2.5	3.7	3.0	2.5
T5	3.7	2.1	3.4	3.0	2.4
G6	3.9	2.3	3.4	3.0	2.5
C13	3.7	2.1	3.3	3.0	2.5
ϵA14	3.9	2.3	3.6	3.0	2.4
C15	3.7	2.2	3.5	3.0	2.4

	interresidue distances on the same strand (Å)				
	H1′–base	H2′–base	H2″–base	base–CH_3	H1′–CH_3
G4–T5	3.3	4.8	3.1	4.8	4.5
T5–G6	3.4	4.3	2.8		
C13–ϵA14	2.8	4.1	2.4		
ϵA14–C15	2.9	4.1	2.4		

	interresidue distances on partner strands (Å)			
	ϵA14(H5)	ϵA14(H8)	ϵA14(H7)	ϵA14(H2)
G4(NH1)	3.5	4.4	2.6	8.2
G6(NH1)	3.8	5.4	4.6	6.1
T5(NH3)	2.4	4.6	2.5	7.9

	interresidue distances on partner strands (Å)			
	G4(NH1)	G6(NH1)	C13(NH_2-4)	C15(NH_2-4)
T5(NH3)	4.2	3.4	4.1, 5.7	6.0, 7.0

[a] Base: H6 protons for pyrimidine, H8 protons for purines, and H2 proton for ϵdA14.

Table V: Proton–Proton Distances in the d(G4-T5-G6)·d(C13-ϵA14-C15) Segment for the Energy-Minimized Structure II of the ϵdA·dT 9-mer Duplex[a]

	intraresidue distances on the same strand (Å)				
	base–H1′	base–H2′	base–H2″	H1′–H2′	H1′–H2″
G4	3.8	2.3	3.3	3.0	2.5
T5	3.7	2.1	3.4	3.0	2.5
G6	3.9	2.4	3.7	3.0	2.5
C13	3.7	2.1	3.2	3.0	2.5
ϵA14	3.9	2.3	3.7	3.0	2.5
C15	3.7	2.2	3.4	3.1	2.5

	interresidue distances on the same strand (Å)				
	H1′–base	H2′–base	H2″–base	base–CH_3	H1′–CH_3
G4-T5	3.1	4.9	3.3	4.3	3.9
T5-G6	2.8	4.2	2.7		
C13-ϵA14	2.8	4.4	2.7		
ϵA14-C15	3.0	3.9	2.5		

	interresidue distances on partner strands (Å)			
	ϵA14(H5)	ϵA14(H8)	ϵA14(H7)	ϵA14(H2)
G4(NH1)	4.5	4.8	4.0	8.3
G6(NH1)	4.1	3.9	3.5	6.2
T5(NH3)	3.5	3.9	2.0	8.8

	interresidue distances on partner strands (Å)			
	G4(NH1)	G6(NH1)	C13(NH_2-4)	C15(NH_2-4)
T5(NH3)	2.9	5.4	6.0, 7.3	5.2, 6.5

[a] Base: H6 protons for pyrimidine, H8 protons for purines, and H2 proton for ϵdA14.

Discussion

In recent years, much progress has been made in using nuclear magnetic resonance spectroscopy as a tool to probe the structural features of nucleic acid adducts inserted at specific sites in DNA oligomer helices [reviewed in Basu and Essigmann (1988) and Harris et al. (1988)]. Our laboratories have undertaken a research program to determine the structural features at exocyclic adduct sites with the goal of coupling this structural information with biological studies performed in parallel toward a better understanding of the molecular basis of the mutagenic events associated with exocyclic nucleic acid lesions. Structural studies on the 1,N^2-propanodeoxyguanosine exocyclic adduct have provided insights into the conformational and base pairing properties of modified lesions in DNA oligomer duplexes and the influences of hydrogen bonding, protonation, and hydrophobic interactions as a function of the pH of the solution (Kouchakdjian et al., 1989, 1990).

Building upon this previous work, we now address the

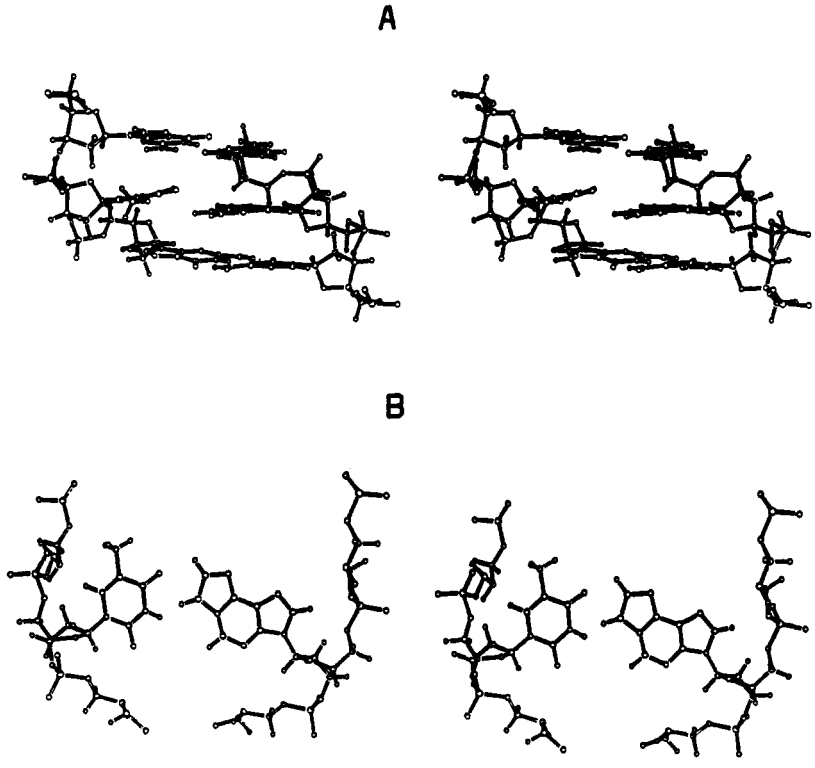

FIGURE 6: Stereopairs of energy-minimized structure II with dT5 displaced toward the dG4·dC15 pair. (A) The d(G4-T5-G6)·d(C13-ϵA14-C15) trinucleotide segment viewed normal to the helix axis and (B) the dT5·ϵdA14 alignment viewed down the helix axis in the ϵdA·dT 9-mer duplex.

structural questions related to the positioning of the 1,N^2-ethenodeoxyadenosine opposite thymidine in the center of a nonanucleotide duplex. Our approach involves using two-dimensional NMR techniques to assign the majority of the proton resonances in the ϵdA·dT 9-mer duplex in both H_2O and D_2O solution. The NOE-based proton–proton distance constraints can be analyzed to identify structural features and pairing alignments at the exocyclic lesion site.

General Features of the ϵdA·dT 9-mer Duplex. The base pairing characteristics of an ϵdA·dT 9-mer may be deduced from analysis of the NOESY spectra in H_2O. The observed NOEs between the thymidine imino and deoxyadenosine H2 protons establish Watson–Crick pairing for the dA2·dT17, dT3·dA16, dT7·dA12, and dA8·dT11 pairs (Figure 2A). Similarly, the NOEs between the deoxyguanosine imino and the hydrogen-bonded and exposed deoxycytidine amino protons confirm Watson–Crick pairing for the dG4·dC15 and dG6·dC13 pairs that immediately flank the dT5·ϵdA14 lesion site (Figure 2A).

The base stacking and handedness of the duplex can be determined from the pattern of NOE cross peaks between base–sugar and base–base protons of adjacent nucleotide units in the ϵdA·dT 9-mer duplex. The observed NOEs between the base (purine H8 or pyrmidine H6) protons and their own and 5′-linked sugar H1′ (Figure 4) and H2′ and H2″ (Figure 5A) protons and between adjacent base protons in purine H8/pyrimidine H6 (3′–5′) pyrimidine H5/CH_3 steps (Figures 4 and 5) are consistent with the ϵdA·dT 9-mer adopting a right-handed helix with all bases being stacked into the duplex.

A comparison of the NOE cross peak intensities of the base to its own sugar H1′ protons (too weak to detect) with those between the cytidine H6 and H5 protons (fixed distance of 2.45 Å) in NOESY spectra recorded at a 50-ms mixing time (Figure S2B) establishes that all nucleotide glycosidic torsion angles are in the anti range in the ϵdA·dT 9-mer duplex.

The 11.10 ppm Resonance. Our one-dimensional NOE data on the ϵdA·dT 9-mer duplex (Figure 3) are consistent with the 11.10 ppm exchangeable resonance originating in the imino proton of dT5, which is positioned opposite the ϵdA14 exocyclic adduct site. We currently have no explanation for the observed intensity in excess of one proton for this resonance, especially at low pH (Figure S1). The excess intensity at 11.10 ppm introduces uncertainties in the interpretation of the one-dimensional NOE difference spectra recorded on the ϵdA·dT 9-mer duplex in H_2O solution (Figure 3).

dT5(anti)·ϵdA14(anti) Alignment. The alignment of the dT5 and ϵdA14 at the lesion site was determined following analysis of the NOE-based distance constraints deduced from the two-dimensional NOESY data sets on the ϵdA·dT 9-mer duplex in H_2O and D_2O solution. We can readily establish that ϵdA14 at the lesion site stacks into the helix in an anti orientation between the dG4·dC15 and dG6·dC13 base pairs since NOEs are observed between the H5, H7, and H8 protons of ϵdA14 and the imino protons of dG4 and dG6 in the ϵdA·dT 9-mer duplex (Figure 2A). Furthermore, dT5 at the dT5·ϵdA14 lesion site also stacks in an anti orientation into the helix since its imino proton exhibits an NOE to the H5 of ϵdA14 and the imino proton of dG4 (Figure 3).

Energy-Minimized Structures. The six initial starting models incorporated dT5(anti) and ϵdA14(anti) alignments at the lesion site, and the energy minimization runs were guided by the interproton distance bounds deduced from the volume integrals of the NOE cross peaks by using the two-spin approximation.

The starting model with dT5 and ϵdA14 displaced toward their 3′ neighbors (Init 6) and four other starting models (Init 1–4) all refined to a common conformation, structure I, with dT5 displaced toward the dG6·dC13 base pair (Figure S3). The starting model with dT5 and ϵdA14 displaced toward their 5′neighbors (Init 5) refined to structure II with retention of the displacement of dT5 toward the dG4·dC15 base pair (Figure 6).

The distance restraints with wide bounds involving nonexchangeable protons for the d(G4-T5-G6)·d(C13-ϵA14-C15)

segment (Table III), which reflect formation of a right-handed helix with anti glycosidic bonds, are satisfied by the energy-minimized structures I (Table IV) and II (Table V). We can differentiate between structures I and II on the basis of constraints between exchangeable protons on adjacent base pairs within the d(G4-T5-G6)·d(C13-ϵA14-C15) segment that were not included in the constraints data set used in the energy minimization computation. The dT5(NH3) proton is closer to the dG4(NH1) proton relative to the dG6(NH1) proton in structure II (Table V), and the reverse holds for structure I (Table IV). Experimentally, the dT5(NH3) proton exhibits an NOE only to the dG4(NH1) proton (Figure 3) consistent with the interproton distances for structure II and not structure I. Similarly, the dT5(NH3) proton is closer to the hydrogen-bonded dC15(NH_2) proton relative to the hydrogen-bonded dC13(NH_2) proton in structure II (Table V), and the reverse holds for structure I (Table IV). Experimentally, the dT5(NH3) proton exhibits an NOE only to the hydrogen-bonded dC15(NH_2) proton (Figure 3) consistent with the interproton distances for structure II and not structure I.

The dT5(anti) and ϵdA14(anti) bases, though not in the same plane, are directed toward the helix axis in structures I (Figure S3) and II (Figure 6). The interproton separations between the NH3 proton of dT5 and the H7 and H8 protons of ϵdA14 are short in structure II (Table V) and in structure I (Table IV). The predicted NOEs between the NH3 proton of dT5 and the H7 (7.32 ppm) and H8 (6.75 ppm) protons of ϵdA14 were not detected in the one-dimensional NOE difference spectrum of the ϵdA·dT 9-mer duplex (Figure 3). We have no explanation for this discrepancy though it is likely that the 6.75 ppm H8 proton of ϵdA14, which is closest to the H_2O resonance and to a lesser extent the 7.32 ppm H7 proton of ϵdA14, will have their intensities attenuated by the shape of the water suppression pulse. A weak NOE is detected between the NH3 proton of dT5 and the 8.72 ppm H5 proton of ϵdA14 (Figure 3) consistent with the <4.5 Å interproton separation predicted for structures I (Table IV) and II (Table V).

We detect weak cross peaks between the H5 proton of ϵdA14 and the imino protons of dG4 (peak K, Figure 2A) and dG6 (peak J, Figure 2A) and between the H7 proton of ϵdA14 and the imino proton of dG4 (peak M, Figure 2A) and dG6 (peak L, Figure 2A) in the NOESY spectrum of the ϵdA·dT 9-mer duplex. These NOEs are consistent with the corresponding interproton distances listed for structure II (Table IV). By contrast, we do not experimentally detect the strong NOE between the imino proton of dG4 and the H7 proton of ϵdA14 corresponding to the interproton separation of 2.6 Å predicted for structure I (Table IV).

These comparisons between the experimental one-dimensional (Figure 3) and two-dimensional (Figure 2) NOE parameters in the d(G4-T5-G6)·d(C13-ϵA14-C15) segment with predicted distances (Table IV) for structure I (Figure S3) and predicted distances (Table V) for structure II (Figure 6) favor the latter conformation for the ϵdA·dT 9-mer duplex.

The conformation of the d(G4-T5-G6)·d(C13-ϵA14-C15) segment in the energy-minimized structure II which satisfies the majority of the experimental distance restraints establishes that dT5 and ϵdA14 are not in the same plane with the dT5 base displaced toward the dG4·dC15 base pair (Figure 6). There is no hydrogen bonding between dT5 and ϵdA14, and the alignment must therefore be stabilized by stacking interactions between the dT5 and ϵdA14 bases at the lesion site and the flanking dG4·dC15 and dG6·dC13 base pairs in the ϵdA·dT 9-mer duplex.

Conclusion. We have applied high-resolution two-dimensional NMR spectroscopy to elucidate structural features of the alignment of dT5 opposite ϵdA14 in the ϵdA·dT 9-mer duplex. Our NMR studies establish that both dT5 and ϵdA14 adopt anti orientations and are directed into the interior of a right-handed helix without disruption of the flanking dG4·dC15 and dG6·dC13 base pairs. Our energy minimization computations starting from a range of different alignments of dT5 and ϵdA14 resulted in structures where these bases at the lesion site are displaced in opposite directions toward flanking dG·dC base pairs. The NMR data are in better agreement with an energy-minimized structure where dT5 is displaced toward the dG4·dC15 base pair rather than the dG6·dC13 base pair. Thus, the ϵdA adduct in an anti orientation can be positioned opposite thymidine in an anti orientation in a DNA duplex with the potential steric clash relieved by the noncoplanar alignment of ϵdA14 and dT5 across the lesion site.

ACKNOWLEDGMENTS

NMR studies were undertaken on instruments purchased with funds provided by the Robert Woods Johnson, Jr., Charitable Trust and Matheson Foundation.

SUPPLEMENTARY MATERIAL AVAILABLE

Figure S1, showing the exchangeable proton NMR spectra of the ϵdA·dT 9-mer duplex at pH 7.0 and 5.2, Figure S2, showing (A) the 250-ms mixing time NOESY contour plot of this duplex in D_2O and (B) an expanded contour plot of the 50-ms mixing time NOESY spectrum for this duplex, and Figure S3, showing stereopairs of energy-minimized structure I with dT5 displaced toward the flanking dG6·dC13 base pair (4 pages). Ordering information is given on any current masthead page.

REFERENCES

Barbin, A., Bartsch, H., Leconte, P., & Radman, M. (1981) *Nucleic Acids Res. 9*, 375–387.

Barrio, J. R., Secrist, J. A., III, & Leonard, N. J. (1972) *Biochem. Biophys. Res. Commun. 46*, 597–604.

Basu, A. K., & Essigmann, J. M. (1988) *Chem. Res. Toxicol. 1*, 1–18.

Basu, A. K., Niedernhofer, L. J., & Essigmann, J. M. (1987) *Biochemistry 26*, 5626–5635.

Creech, J. L., & Johnson, M. N. (1974) *J. Occup. Med. 16*, 150–151.

Gaffney, B. L., & Jones, R. A. (1989) *Biochemistry 28*, 5881–5889.

Gait, M. J. (1984) *Oligonucleotide Synthesis: A Practical Approach*, IRL Press, Washington, DC.

Green, T., & Hathway, D. E. (1978) *Chem.-Biol. Interact. 22*, 211–224.

Guengerich, F. P., Crawford, W. M., Jr., & Watanabe, P. L. (1979) *Biochemistry 18*, 5177–5182.

Hall, J. A., Saffhill, R., Green, T., & Hathway, D. E. (1981) *Carcinogenesis 2*, 141–146.

Hare, D. R., Wemmer, D. E., Chou, S. H., Drobny, G., & Reid, B. R. (1983) *J. Mol. Biol. 171*, 319–336.

Harris, T. M., Stone, M. P., & Harris, C. M. (1988) *Chem. Res. Toxicol. 1*, 79–96.

Kouchakdjian, M., Marinelli, E., Gao, X., Johnson, F., Grollman, A., & Patel, D. (1989) *Biochemistry 28*, 5647–5657.

Kouchakdjian, M., Eisenberg, M., Live, D., Marinelli, E., Grollman, A. P., & Patel, D. J. (1990) *Biochemistry 29*, 4456–4465.

Kusmierek, J. T., & Singer, B. (1982) *Biochemistry 21*, 5717-5722.
Laib, R. J., & Bolt, H. M. (1977) *Toxicology 8*, 185-195.
Laib, R. J., Gwinner, L. M., & Bolt, H. M. (1981) *Chem.-Biol. Interact. 37*, 219-231.
Leonard, N. J. (1984) *CRC Crit. Rev. Biochem. 15*, 125-199.
Osterman-Golkar, S., Hultmark, D., Segerback, D., Calleman, C. J., Gothe, R., Ehrenberg, L., & Wachtmeister, C. A. (1977) *Biochem. Biophys. Res. Commun. 76*, 259-266.
Sattsangi, P. D., Leonard, N. J., & Frihart, C. R. (1977) *J. Org. Chem. 42*, 3292-3296.
Scherer, E., Van Der Laken, C. J., Gwinner, L. M., Laib, R. J., & Emmelot, P. (1981) *Carcinogenesis 2*, 671-677.
Secrist, J. A., III, Barrie, J. R., Leonard, N. J., & Weber, G. (1972) *Biochemistry 11*, 3499.
Singer, B., & Grunberger, D. (1983) *Molecular Biology of Mutagens and Carcinogens*, Plenum Press, New York.
Singer, B., & Bartsch, H., Eds. (1986) *The Role of Cyclic Nucleic Acid Adducts in Carcinogenesis and Mutagenesis*, IARC Scientific Publications 70, IARC, Lyon, France.
Singer, B., & Spengler, S. J. (1986) in *The Role of Cyclic Nucleic Acid Adducts in Carcinogenesis and Mutagenesis* (Singer, B., & Bartsch, H., Eds.) IARC Scientific Publications 70, pp 359-371, IARC, Lyon, France.
Singer, B., Abbott, L. G., & Spengler, S. J. (1984) *Carcinogenesis 5*, 1165-1171.
Singer, B., Spengler, S. J., Chavez, F., & Kusmierek, J. T. (1987) *Carcinogenesis 8*, 745-747.
Spengler, S., & Singer, B. (1981) *Nucleic Acids Res. 9*, 365-373.

NMR Studies of the Exocyclic 1,N^6-Ethenodeoxyadenosine Adduct (ϵdA) opposite Deoxyguanosine in a DNA Duplex. ϵdA(syn)·dG(anti) Pairing at the Lesion Site†

Carlos de los Santos,‡ Michael Kouchakdjian,‡ Kevin Yarema,§ Ashis Basu,§ John Essigmann,*,§ and Dinshaw J. Patel*,‡

Department of Biochemistry and Molecular Biophysics, College of Physicians and Surgeons, Columbia University, New York, New York 10032, and Department of Chemistry and Whitaker College of Health Sciences and Technology, Massachusetts Institute of Technology, Cambridge, Massachusetts 02139

Received September 6, 1990; Revised Manuscript Received October 29, 1990

ABSTRACT: Proton NMR studies are reported on the complementary d(C-A-T-G-G-G-T-A-C)·d(G-T-A-C-ϵA-C-A-T-G) nonanucleotide duplex (designated ϵdA·dG 9-mer duplex), which contains the exocyclic adduct 1,N^6-ethenodeoxyadenosine positioned opposite deoxyguanosine in the center of the helix. The present study focuses on the alignment of dG5 and ϵdA14 at the lesion site in the ϵdA·dG 9-mer duplex at neutral pH. This alignment has been characterized by monitoring the NOEs originating from the NH1 proton of dG5 and the H2, H5, and H7/H8 protons of ϵdA14 in the central d(G4-G5-G6)·d(C13-ϵA14-C15) trinucleotide segment of the ϵdA·dG 9-mer duplex. These NOE patterns establish that ϵdA14 adopts a syn glycosidic torsion angle that positions the exocyclic ring toward the major groove edge while all the other bases including dG5 adopt anti glycosidic torsion angles. We detect a set of intra- and interstrand NOEs between protons (exchangeable and nonexchangeable) on adjacent residues in the d(G4-G5-G6)·d(C13-ϵA14-C15) trinucleotide segment which establish formation of right-handed helical conformations on both strands and stacking of the dG5(anti)·ϵdA14(syn) pair between stable dG4·dC15 and dG6·dC13 pairs. The energy-minimized conformation of the central d(G4-G5-G6)·d(C13-ϵA14-C15) segment establishes that the dG5(anti)·ϵdA14(syn) alignment is stabilized by two hydrogen bonds from the NH1 and NH_2-2 of dG5(anti) to N9 and N1 of ϵdA14(syn), respectively. The NH1 proton of dG5 resonates at 14.0 ppm, and its downfield shift is consistent with hydrogen bond formation with the ring nitrogen (N9) of ϵdA14 at the lesion site in the ϵdA·dG 9-mer duplex. The H6 and H5 base protons of dC13 and dC15 are broad in the ϵdA·dG 9-mer duplex, with some broadening also observed at the H2 and H5 base protons of ϵdA14 in NMR spectra recorded at ambient temperature. The observed broadening may originate in conformational averaging among ϵdA14 alignments on the intermediate time scale, which would affect the stacking in the d(C13-ϵA14-C15) segment centered about the lesion site. In summary, the dG5(anti)·ϵdA14(syn) alignment is readily accommodated into the DNA helix without disruption of flanking dG4·dC15 and dG6·dC13 base pairs and may account for the incorporation of dG opposite ϵdA during in vitro replication by DNA polymerase I.

There is currently very little known at the molecular level about structural features of nucleic acid exocyclic adducts important in mutagenesis and carcinogenesis (Singer & Bartsch, 1986). The formation of these adducts not only interferes with base pairing regions of nucleic acid components but also induces substantial alterations in the pK_a and hydrophobicity at the lesion site. There is a potential for local helix distortion at exocyclic adduct sites with important consequences on polymerase fidelity and repair efficiency at the lesion site.

Our groups are collaborating on an investigation of the structure and base pairing alignments of the 1,N^6-ethenodeoxyadenosine (ϵdA) exocyclic adduct **1** incorporated in DNA

†This research was supported by NIH Grant CA-49982 to D.J.P. and NIH Grant CA-52127 to J.E. C.d.l.S. was supported by an NIH International Fogarty Fellowship.
‡Columbia University.
§Massachusetts Institute of Technology.

0006-2960/91/0430-1828$02.50/0